Chemically distinct transition states govern rapid dissociation of single L-selectin bonds under force

Evan Evans[†‡§], Andrew Leung[†], Dan Hammer[¶], and Scott Simon[‖]

[†]Departments of Physics and Pathology, University of British Columbia, Vancouver, BC, Canada V6T 2A6; [‡]Department of Biomedical Engineering, Boston University, Boston, MA 02215; [¶]Department of Biomedical Engineering, University of Pennsylvania, Philadelphia, PA 19104; and [‖]Department of Biomedical Engineering, University of California, Davis, CA 95616

Edited by Yuan-Cheng B. Fung, University of California at San Diego, La Jolla, CA, and approved January 16, 2001 (received for review July 13, 2000)

Carbohydrate–protein bonds interrupt the rapid flow of leukocytes in the circulation by initiation of rolling and tethering at vessel walls. The cell surface carbohydrate ligands are glycosylated proteins like the mucin P-selectin glycoprotein ligand-1 (PSGL-1), which bind ubiquitously to the family of E-, P-, and L-selectin proteins in membranes of leukocytes and endothelium. The current view is that carbohydrate–selectin bonds dissociate a few times per second, and the unbinding rate increases weakly with force. However, such studies have provided little insight into how numerous hydrogen bonds, a Ca^{2+} metal ion bond, and other interactions contribute to the mechanical strength of these attachments. Decorating a force probe with very dilute ligands and controlling touch to achieve rare single-bond events, we have varied the unbinding rates of carbohydrate–selectin bonds by detachment with ramps of force/time from 10 to 100,000 pN/sec. Testing PSGL-1, its outer 19 aa (19FT), and sialyl Lewis^X (sLe^X) against L-selectin *in vitro* on glass microspheres and *in situ* on neutrophils, we found that the unbinding rates followed the same dependence on force and increased by nearly 1,000-fold as rupture forces rose from a few to ≈200 pN. Plotted on a logarithmic scale of loading rate, the rupture forces reveal two prominent energy barriers along the unbinding pathway. Strengths above 75 pN arise from rapid detachment (<0.01 sec) impeded by an inner barrier that requires a Ca^{2+} bond between a single sLe^X and the lectin domain. Strengths below 75 pN occur under slow detachment (>0.01 sec) impeded by the outer barrier, which appears to involve an array of weak (putatively hydrogen) bonds.

Invariably challenged by physical stresses, adhesive interactions in biology involve a dynamic struggle between bond formation and rupture. Nowhere is this competition more intense than when leukocytes patrol and stick to vessel walls in the circulation. In the process of recognition, the full hydrodynamic force of the flow is applied to the linkage between blood cell and endothelium within milliseconds. The crucial physical requirement for the bonding interaction is to provide high strength under fast loading but to still release quickly if there is no local need for cell capture. This well-known (1–5) specialized function is accomplished by calcium-dependent bonds between the family of L-, P-, and E-selectin protein receptors and their complex carbohydrate-like ligands [e.g., GlyCAM1, CD34 and podocalyxin, P-selectin glycoprotein ligand-1 (PSGL-1), and ESL-1]. The best characterized ligand is PSGL-1, a leukocyte mucin that binds to the outer lectin domain of all of the selectins and depends on Ca^{2+}. The interactions involve fucosylated and sialylated oligosaccharides related to the tetrasaccharide sialyl Lewis X (sLe^X), which are added by posttranslational modifications to PSGL-1 at many O-linked sites along each branch of the homodimer (6–8). Also affecting the interactions, posttranslational sulfation can occur at three tyrosine residues in the outer 19 aa of mature PSGL-1 along with a single O-linked site for sLe^X (8). Indeed, the short 19-aa region appears sufficient for binding to P- and L-selectin provided that an sLe^X-modified O-linked oligosaccharide is present at Thr-16 (8, 9) and at least one of the three tyrosines is sulfated (9). Recently, crystal structures were obtained for cocomplexes of sLe^X with constructs of E- and P-selectin as well as cocomplexes of the N-terminal domain of PSGL-1 (modified by both tyrosine sulfation and sLe^X) with P-selectin (10). The structures reveal largely electrostatic interactions (hydrogen bonds, water bridges, and a Ca^{2+} metal ion bond) between the lectin domain and the fucosylated (FT) ligands (10). Although generically similar in the sites of binding to sLe^X and of calcium to fucose, the interactions between sLe^X and PSGL-1 bonds to P- and E-selectin differ in subtle but important ways, including the coordination of Ca^{2+} (10).

Selectin- and carbohydrate-mediated attachment of cells or particles to carbohydrate- and selectin-decorated substrates in flow channel experiments have been used extensively to model the physiological phenomena of leukocyte rolling and tethering observed in the microcirculation of living animals (1–5, 8, 11–16). Most relevant here, tethering refers to the transient capture of cells under constant wall shear stress. Derived from the decay in number of attached cells with time, the detachment rate is thought to reveal single-bond kinetics. For wild-type PSGL-1 interactions with L-selectin, detachment rates start at 10 per second under forces of 40–60 pN and typically increase only to 20–30 per sec (9, 13, 14) when forces reach 200–300 pN [a notable exception (16) will be discussed later]. Furthermore, mutations that diminish tyrosine sulfation in the N-terminal region of PSGL-1 lead to a fewfold increase in cell detachment rate, and attachments are wiped out if sLe^X is eliminated from this region (9). From these studies it is concluded that the increase in rate of cell detachment under force reflects exponentiation of single-bond kinetics governed by a large force scale $f_\beta \approx 200$ pN, i.e., $k_{off} \approx 1/t_{off} \exp(f/f_\beta)$, with $1/t_{off} \approx 7$–10 per sec. According to Bell (17), the thermal force scale f_β is believed to be set by the ratio of thermal energy k_BT to a very small molecular length x_β (0.2Å) intrinsic to a single activation barrier or thermodynamic transition state, i.e., $f_\beta = k_BT/x_\beta$. By comparison, PSGL-1 bonds to P-selectin were pulled apart with an atomic force microscope (18) and found to dissociate 20–100 times faster than in flow chamber tests (9, 12) at the same levels of force (120–170 pN). Even though the atomic force microscope measurements only covered a 20-fold span in speed of detachment, the unbinding rate appeared to be exponentiated on a

This paper was submitted directly (Track II) to the PNAS office.

Abbreviations: BFP, biomembrane force probe; PSGL-1, P-selectin glycoprotein ligand-1; FT, fucosylated; sLe^X, sialyl Lewis X; sLe^X, biotinylated sLe^X; PMN, polymorphonuclear leukocyte; PEG, polyethylene glycol.

[§]To whom reprint requests should be addressed at: Department of Physics and Astronomy, University of British Columbia, Vancouver, BC, Canada V6T 2A6. E-mail: evans@physics.ubc.ca.

The publication costs of this article were defrayed in part by page charge payment. This article must therefore be hereby marked "*advertisement*" in accordance with 18 U.S.C. §1734 solely to indicate this fact.

www.pnas.org/cgi/doi/10.1073/pnas.061324998

force scale an order of magnitude lower ($f_\beta \approx 16$ pN), and extrapolation to zero force implied a 50-fold slower unstressed rate of dissociation ($1/t_{off} \approx 0.02$ per sec) than deduced from flow chamber studies. Thus, the kinetic profile for unbinding a single carbohydrate–selectin bond under force and the landscape of energy barriers that governs bond strength remained in question.

In this work, we have measured the mechanical strengths of single L-selectin bonds to PSGL-1, its outer 19-aa segment (19FT), and sLe^X over many decades in rupture time. For detachment under a large range of loading rates (force/time), the measurements of bond strength on a scale of log(loading rate) provide a spectroscopic image of prominent energy barriers traversed along the force-driven reaction coordinate (19–21). In this way, dynamic force spectroscopy exposes barriers (especially inner barriers) that are difficult or impossible to detect in solution assays of near-equilibrium dissociation. The dynamic force spectroscopy concept has been used by us to explore energy landscapes of biotin·(strept)avidin bonds (22) and lipid anchoring in membranes (23) and by others to characterize domain unfolding in muscle titin (24) and in the extracellular matrix protein tenascin (25), and separation of strands in short DNA oligomers (26) and of homotypic bonds between cadherins (27). Because of the inherent logarithmic dependence of rupture force on speed of loading, the dynamic force spectroscopy method is most revealing when applied over many orders of magnitude in loading rate. For this reason, we have used a biomembrane force probe (BFP) (22, 28) with a dynamic range from ≈0.1 pN/sec to 10^5 pN/sec and a span of force from <1 pN to 1 nN to test carbohydrate–selectin interactions. Probing bonds to L-selectin on glass microspheres and *in situ* on leukocytes, we have found an unexpected hierarchy of two transition states that correlate with specific chemical features of PSGL-1 and govern the enormous amplification in rate of bond dissociation that arises under force.

Materials and Methods

Carbohydrate Ligands, L-Selectin, and Blocking Antibodies. Recombinant forms of human PSGL-1, the outer 19-aa segment (19FT) of mature PSGL-1, and human L-selectin (L-sel) were generous gifts from Ray Camphausen at the Genetics Institute (Cambridge, MA). A biotinylated construct of the tetrasaccharide sialyl $Lewis^X$ ($bsLe^X$) was purchased from GlycoTech (Rockville, MD). As described (6, 8), the recombinant PSGL-1 consisted of the entire extracellular domain in the form of a disulfide-linked homodimer, whereas 19FT was a chimera derived from fusion to a human IgG Fc domain. Plasmids encoding PSGL-1 and the truncated 19-mer chimera were transfected in Chinese hamster ovary cells along with $\alpha(1,3/1,4)$-fucosyltransferase-VII enzyme (6). Similarly, the L-selectin was a chimeric construction with the N-terminal and epidermal growth factor domains plus two consensus repeat motifs fused to a human IgG Fc domain. Plasmids encoding the chimeric form of L-selectin were also transfected into Chinese hamster ovary cells. The secreted materials were purified from serum-free media by conventional chromatography (6, 8). Antibodies to L-selectin (DREG 55 and DREG 200) were human IgGs generously provided by Protein Design Laboratories (Mountain View, CA). An antibody to PSGL-1 (KPL1) was generously provided by Geoffrey Kansas at Northwestern University (Evanston, IL).

Immobilization of Ligands and Receptors on Microspheres. A common procedure was used to covalently link biotin and constructs of PSGL1 or L-selectin to glass microspheres. Borosilicate spheres (Duke Scientific, Palo Alto, CA) with ≈1- to 2-μm diameters were chosen for probe tips to be decorated with PSGL-1, 19FT, or $bsLe^X$, and spheres with ≈4- to 5-μm diameters were chosen for receptor targets to be decorated with L-selectin. After cleaning in a mixture of ammonium hydroxide–hydrogen peroxide–water at boiling temperature and washing, mercaptosilane groups [3-mercaptopropyltrimethoxysilane (MPTMS); United Chemical Technologies, Bristol, PA] were attached to the spheres. For preparation of BFP tips with PSGL-1 and 19FT, the mercaptosilanized spheres were reacted with a mixture of heterobifunctional polyethylene oxide (polyethylene glycol, PEG) polymers (VS-PEG3400-NHS plus maleimide-PEG3400-biotin in a ratio of 1:20; VS indicates vinyl sulfone and NHS indicates *N*-hydroxysuccinimide; Shearwater Polymers, Huntsville, AL) to fix many biotin groups and a small number of sites for the ligands. To further dilute the specific sites, a VS-PEG2000-VS was included in a ratio of 5:1 to the two other PEG linkers and capped by cysteine. The final ratio of ligand sites to total PEG linkages was ≈1:100. The spheres were then washed, and the ligand was reacted with the remaining NHS group of the VS-PEG-NHS linkage. Finally, the biotinylated/ligand-decorated spheres were saturated with streptavidin (Pierce) and washed to prepare for assembly with a biotinylated BFP capsule. To decorate tips with sLe^X, streptavidin/PEG-biotinylated spheres were exposed to a very dilute solution of $bsLe^X$, which was further diluted as needed with an admixture of biotinylated nonspecific IgG. Similarly, the L-selectin chimera was covalently attached to the larger silanized spheres with the use of VS-PEG3400-NHS and VS-PEG2000-VS. No biotin was present on the target surface.

Neutrophils. Fresh human blood samples were collected by venipuncture into a sterile syringe containing 10 units/ml heparin (Elkins-Sinn, Cherry Hill, NJ). After low-speed centrifugation to remove red cells, polymorphonuclear leukocytes (PMNs) were concentrated with the use of Mono-Poly resolving medium (ICN). The isolated PMNs were kept at 4°C in Ca^{2+}-free Hepes buffer (110 mM NaCl/10 mM KCl/10 mM glucose/1 mM $MgCl_2$/30 mM Hepes, pH 7.35) containing 0.1% human serum albumin (Armour Pharmaceutical) until use within 4 h.

The BFP Transducer and Dynamic Force Measurements. For use as BFP transducers, human red cells were covalently linked with PEG-biotin polymers with the use of the heterobifunctional amine reactive NHS-PEG3400-biotin (Shearwater Polymers). Once biotinylated, a red cell capsule and streptavidinated ligand-decorated sphere were selected by micromanipulation and maneuvered to form strong adhesive contact. Pressurized by micropipette aspiration (pressure ΔP and inner radius R_p), the red cell capsule–sphere assembly became a BFP (28). Proportional to membrane tension ($\approx \Delta P R_p$), the force constant k_f (force/capsule extension) was accurately set in the range of 0.1–2 pN/nm by choosing the pipette suction. Operated on the stage of an inverted microscope, the BFP (at left in Fig. 1 *A* and *B*) was kept stationary. Also held by micropipette, a PMN (at *Right* in Fig. 1*A*) or L-selectin sphere (at right in Fig. 1*B*) was translated to/from contact with the BFP by precision-piezo displacements. With fast video processing (≈1,500 frames per sec), a simulated cursor was required to track the trailing edge of the probe tip as illustrated in Fig. 1 *A* and *B*, which yielded a resolution δx_p of ≈7 nm at time intervals of 0.0007 sec. The difference between piezo translation and tip displacement was multiplied by the force constant to obtain the elastic force applied to the BFP. Without data averaging, the BFP method spans forces from ≈0.5 pN to >1,000 pN with a sensitivity of ≈0.2 pN at 1 pN and ≈10 pN at 1,000 pN. An important attribute of the BFP system is that it can cover a millionfold range in loading rate. The loading rate r_f ($= \Delta f/\Delta t$) is the product of the force constant (for the transducer coupled with the molecular linkage, which in most cases reduces to the low BFP stiffness) and the speed of separation v_s, i.e., $r_f \approx k_f v_s$. With piezo retraction at speeds from

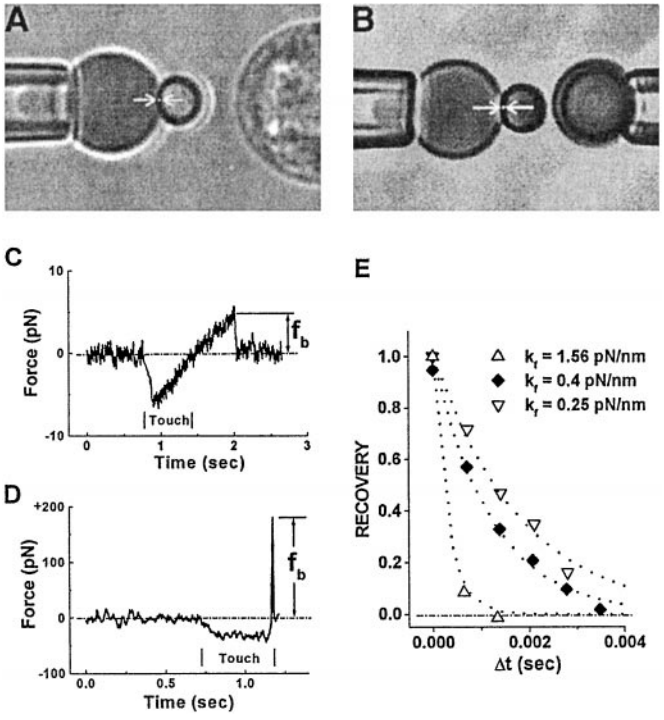

Fig. 1. (*A* and *B*) With ≈2-μm glass spheres as tips decorated by a carbohydrate ligand, BFPs at the left in both images were kept stationary. The targets, a PMN at the right in *A* and an L-selectin tethered sphere at the right in *B*, were translated to/from contact with the BFP at speeds from 1 to 50,000 nm/sec. The BFP spring was a pressurized red blood cell capsule (28). Controlled by micropipette suction, capsule membrane tension was preselected to set the force constant k_f between 0.1 and 2 pN/nm. With ultrafast video processing (≈1,500 frames per sec), a simulated cursor (white dot between arrows) tracked movement of the BFP tip at a resolution of 5–7 nm. (*C* and *D*) Traces of BFP force over time for approach (touch under feed back control) and retraction of a PMN. The rise in force shows the loading up to the maximum BFP elastic force f_b at bond rupture. (*C*) A bond loaded slowly at ≈10 pN/sec held the tip to the surface for ≈1 sec and broke at $f_b \approx 10$ pN. (*D*) A bond loaded at ≈50,000 pN/sec held the tip to the surface for ≈0.003 sec and broke at $f_b \approx 170$ pN. (*E*) BFP recovery at 0.00067-sec intervals after bond rupture for different values of stiffness k_f; extension is normalized by the maximum BFP stretch at $\Delta t = 0$. Dotted lines show the decay defined by $\exp(-k_f \Delta t/\zeta_p)$ and the ratio of stiffness to the damping coefficient $\zeta_p = 0.00048$ pN·sec/nm.

1 nm/sec to 50,000 nm/sec, loading rates can be selected in a range from ≈0.1 to 100,000 pN/sec.

Under ultrafast detachment ($v_s > 30{,}000$ nm/sec), damping of the probe ζ_p (pN·sec/nm) begins to add a hidden viscous force $f_v = v_s\zeta_p$ to the elastic force $f_e = k_f\Delta x$ revealed by transducer stretch Δx. Because deformations of the pressurized BFP capsule are small (<4%), damping is dominated by dissipation in the adjacent liquids. The approximation for small dipolar distortions of a sphere predicts that $\zeta_p \approx 8\pi(\eta_c + \eta_w)r_c$ [i.e., ≈0.0003 pN·sec/nm based on $r_c \approx 3$ μm for the radius of the BFP capsule and $(\eta_c + \eta_w) \approx 4$ centipoise (mN·sec/m^2) for the combined viscosity of the red cell interior plus exterior buffer]. Because the approximation for transducer damping is not accurate enough to be used as a correction factor, we measured the viscous recovery after bond rupture at different values of BFP stiffness to determine the coefficient. When unloaded, recovery is retarded by both transducer damping and hydrodynamic coupling to the target; but for small targets and initial separation by PEG linkers, coupling to the target is imperceptible in the recovery. As demonstrated in Fig. 1*E*, the single-exponential decay in time provided the ratio of damping to stiffness (ζ_p/k_f). Consistent with little variation in radii of the aspirated red cells and in red cell hemoglobin concentrations, the damping coefficient of $\zeta_p \approx 0.00048$ pN·sec/nm was found to be effectively constant and could be used to correct the probe force at each speed v_s of detachment through the relations $f_v = v_s\zeta_p$ and $f = f_e + f_v$. With values of damping ζ_p and position resolution δx_p, optimum sensitivity of the BFP at fast rates of loading r_f (>1,000 pN/sec) is achieved by setting the stiffness to a value of $k_f = (r_f\zeta_p/\delta x_p)^{1/2} \approx 0.008 r_f^{1/2}$.

Measurements of Bond Strength. Decorated by PSGL-1, 19FT, or bsLe^X, a BFP was used to initiate and test bonds to L-selectin on PMN surfaces and on glass spheres. Interactions in Ca^{2+} were tested in a microscope chamber that contained Hanks' buffer plus 1 mM $CaCl_2$. For interactions in a Ca^{2+}-free environment, the tests were performed in a Ca^{2+}- and Mg^{2+}-free buffer plus 10–20 mM EDTA. Probe tips and test spheres were decorated with a very low density of specific sites (one PEG-tethered ligand or receptor per 100 tethered PEG chains produced densities below the detection limit of ≈40 per square micrometer in our fluorescence assay). To achieve a high probability (≥0.9) of rare discrete bond events, a low frequency of tip surface attachments (<1 per 10 touches) was maintained by feedback control of surface contact. At a particular rate of loading, impingement force and duration of contact were preset in the range of 10–40 pN and 0.001–1 sec, respectively, and then kept constant for every touch to a test surface. Examples of touch feedback followed by slow and fast bond detachment are demonstrated in Fig. 1 *C* and *D*. Under touch feedback, each contact became an equivalent event, and the likelihood of discrete bond events could be predicted by the frequency of attachment based on the statistics of dilute uncorrelated events. Because of the low frequency of attachment, several hundred cycles of approach–touch–retraction had to be performed at a preset loading rate to obtain a histogram of 50–100 rupture forces. Derived from a Gaussian fit to each force histogram, the most frequent rupture force f^* defines the mechanical strength at each rate of loading r_f.

Controls and Antibody-Blocking Experiments. Several controls were performed under the common conditions of touching force and contact duration to verify specificity. As the reference for comparison, we first set the frequencies of attachment for the specific ligands (PSGL-1, 19FT, bsLe^X) to L-selectin spheres (L-sel) and PMNs at ≈10:100 touches (Fig. 2*A*, top lanes). Then we tested probes decorated with the carbohydrate ligands and L-selectin against completely nonspecific spheres bearing only PEG groups (PSGL-1:PEG, L-sel:PEG, 19FT:PEG, bsLe^X:PEG; Fig. 2*A*, bottom lanes), where attachment frequencies dropped to ≈1 per 100 touches or less. Moreover, as seen in Fig. 2*B*, the few nonspecific forces that remained were small at all rates of loading. In other experiments, we tested PSGL-1 interactions with L-selectin spheres in the presence of blocking antibodies KPL1, which binds proximally to the tyrosine-rich region of the 19-aa tip of mature PSGL-1 (29), plus humanized DREG 55 and DREG 200, which bind to distinct regions of the lectin domain (30). The L-selectin or PSGL-1 spheres were incubated for 30 min in (and were tested in) a Ca^{2+} buffer plus 10 μg/ml DREG 55 (and DREG 200) or KPL1, respectively. When L-selectin spheres were blocked by DREG 55 or DREG 200, the frequencies of PSGL-1 attachments fell to ≈3:100 touches compared with ≈10:100 in the unblocked tests. The frequency of PSGL-1 attachments to L-selectin spheres was less affected by blocking with KPL1 and dropped to only ≈5:100 touches. In comparison, attachment frequencies fell to ≈2:100 in tests of both PSGL-1 and bsLe^X probes against L-selectin spheres in EDTA. As will be described in the section to follow, detachment forces measured in the presence of the blocking antibodies and in EDTA were significantly lower than forces for

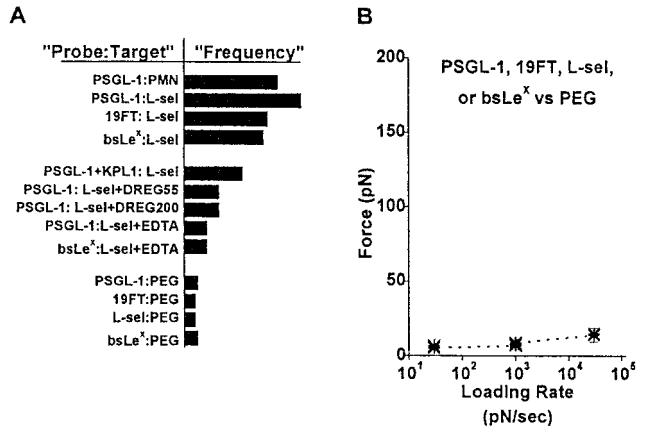

Fig. 2. (*A*) Relative frequencies of attachment for carbohydrate:L-selectin interactions in Ca^{2+} (top four lanes on a scale of ≈1 per 10 touches), in the presence of blocking antibodies and Ca^{2+} or EDTA (middle five lanes), for nonspecific interactions with PEGylated spheres (bottom four lanes), all probed under the fixed conditions of impingement force and contact duration. (*B*) Nonspecific forces (±SD) measured ≈1 per 100 touches to PEGylated microspheres.

the unblocked interactions in Ca^{2+} but remained well above the small nonspecific forces shown in Fig. 2*B*.

Results

Dynamic Force Spectra. We next define force spectra for carbohydrate–L-selectin interactions. The most frequent rupture forces f^* are plotted as functions of log(loading rate) in Fig. 3 *A–C*. With Ca^{2+} present (Fig. 3 *A* and *B*), bond strengths began at 5–10 pN under loading rates of $r_f \approx 10$ pN/sec and followed a sequence of two near-linear dependencies on log(loading rate) to reach ≈200 pN under loading rates of 10^5 pN/sec. Also shown in Fig. 3*A*, the force added by BFP damping was small and contributed only up to ≈15% at the fastest rate of loading. Most striking, spectra for PSGL-1, 19FT, and $bsLe^X$ bonds to L-selectin tethered on spheres in Fig. 3*A* are indistinguishable from the spectrum for 19FT bonds to L-selectin *in situ* on PMNs. Hence bond strength was unaffected by properties of the PMN structure or cell activity, and the recombinant L-selectin was clearly functional when linked to the spheres. Moreover, coincidence of the spectra for attachments of the ligands PSGL-1, 19FT, and $bsLe^X$ to L-selectin indicates that bond strengths were dominated by a link between a single sLe^X group and the lectin domain. Similarly in Fig. 3*B*, nearly identical force spectra were obtained for both the full PSGL-1 homodimer and 19FT attachments to L-selectin on PMNs. Significantly, the steep high-strength regimes of force above 75 pN in Fig. 3 *A* and *B* required Ca^{2+} and vanished when EDTA was added to chelate Ca^{2+} as seen in Fig. 3 *C*. In addition, the high-strength regime was eliminated by the blocking mAbs KPL1, DREG 55, and DREG 200, even with Ca^{2+} present. However, adding EDTA or the blocking mAbs did not eliminate ligand attachments to L-selectin but left similar weak, low-strength regimes shifted to fast loading rates.

Spectra of bond strengths obtained under ramps of force ($f = r_f t$) are easy to interpret when nearly linear regimes of force span decades in log(loading rate = r_f), as seen in Fig. 3 *A–C*. Throughout each regime, a prominent activation barrier or chemical transition state is the dominant impedance to kinetics, and the slope of force versus log(loading rate) maps the barrier to a distance along the direction of force (19). The logarithmic dependence on loading rate stems from exponentiation of the unbinding rate under force. As postulated by Bell (17) and subsequently developed by us in detail (19–21), projection of a

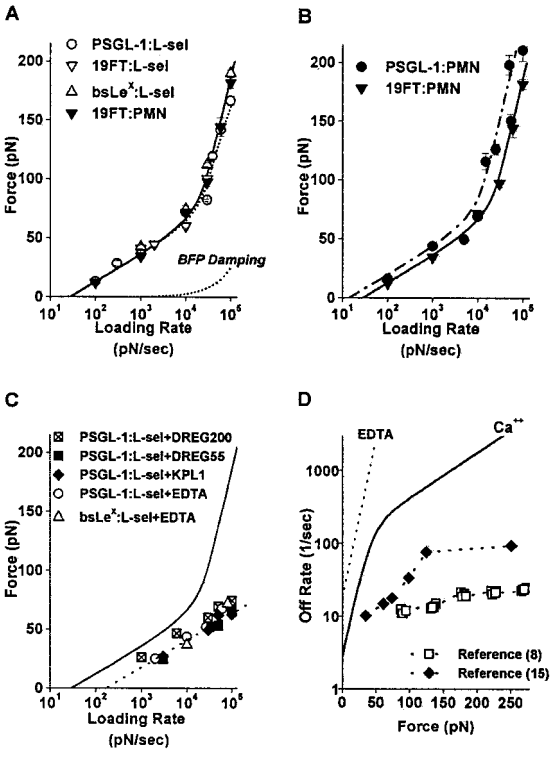

Fig. 3. (*A–C*) The most frequent forces observed to rupture carbohydrate bonds to L-selectin as functions of loading rate. (The values are shown ± standard error in force, which represents the uncertainty in most frequent force; standard deviations in each force histogram were always comparable to the slope of the appropriate linear-like regime, as expected for single bond kinetics.) (*A*) Forces in Ca^{2+} for 19FT attachments to L-selectin *in situ* on PMNs and for PSGL-1, 19FT, $bsLe^X$ attachments to L-selectin *in vitro* on spheres. The lower dotted curve is the correction for viscous damping added to the elastic BFP force illustrated by the upper dotted curve. The solid curve is the continuous spectrum for passage of two energy barriers: an outer barrier at a distance $x_\beta \approx 4$Å along the direction of force with a transition rate $1/t_{off} \approx 3$ per second and an inner barrier at a distance $x_\beta \approx 0.6$Å with a transition rate $1/t_{off} \approx 100$ per sec. (*B*) Forces in Ca^{2+} for PSGL-1 and 19FT attachments to L-selectin *in situ* on PMNs. The solid curve is the spectrum in *A*; the dashed-dotted curve is the spectrum predicted for a zipper of two bonds, where each bond is governed by the solid-curve spectrum. (*C*) Forces in 10–20 mM EDTA for PSGL-1 and $bsLe^X$ attachments to L-selectin on spheres and for PSGL-1 attachments to L-selectin on spheres in Ca^{2+} blocked by mAbs KPL1, DREG55, and DREG200. The solid curve is the spectrum in *A*. (*D*) Kinetic profiles for rate of PSGL-1 dissociation from L-selectin under force in Ca^{2+} (solid curve) and in EDTA or blocked by KPL1 and DREG 55 (dotted curve). Also shown are rates of transient cell detachment observed at different video framing speeds, 30 per sec (9) and 240 per sec (16), in flow chamber studies.

pulling force f along the molecular reaction coordinate x contributes a mechanical potential ($-fx$) that lowers the activation barrier. Because of the Arrhenius-like dependence on energy, exponential amplification of the rate begins when force reaches the scale f_β, where the barrier is lowered by one unit of thermal energy k_BT (4.1×10^{-21} J or 4.1 pN/nm at room temperature). As such, the force level f_β is governed by the thermally averaged distance x_β moved in the direction of force to surmount the barrier, i.e., $f_\beta = k_BT/x_\beta$. Because of exponentiation, the unbinding rate rises rapidly when a ramp of force is applied to a bond, but, as the force continues to rise, the likelihood of bond survival declines precipitously. The crossover between increasing rate of dissociation and decreasing bond survival establishes a peak f^* in the histogram of forces, which defines the strength expected for the bond at the particular loading rate (19). For a hierarchy of activation barriers, the strength spectrum is a

sequence of nearly linear regimes with ascending slopes (20, 21) as seen in Fig. 3 *A–C*. Like a single barrier, each *n*th barrier in the hierarchy is described by an unstressed transition rate $1/t_{off}(n)$ and a force scale $f_\beta(n) = k_BT/x_\beta(n)$ for rate exponentiation again set by its projection $x_\beta(n)$ along the direction of force. The increase in slope $f_\beta(n)$ from one regime to the next signifies that force has become sufficient to suppress an outer barrier and that an inner barrier has emerged to dominate kinetics. In analyzing spectra, we have extended the stationary kinetic rate theory of Kramers (31) to model escape over a series of barriers under force. The outcome is an unbinding rate governed by the sum of times to transit individual barriers (20, 21),

$$k_{off} = 1/\left\{\sum_n t_{off}(n)\exp[-f/f_\beta(n)]\right\}. \quad [1]$$

With an unbinding rate as a function of force, the probability density for rupture events under a ramp of force is described by a Markov process, which predicts the likelihood of bond survival over time. The peak in the distribution is the most frequent force f^* for breakage and is related to the loading rate r_f through the following expression (20, 21):

$$1/r_f = \sum_n [t_{off}(n)/f_\beta(n)]\exp[-f^*/f_\beta(n)]. \quad [2]$$

Immediately apparent for a single barrier with $k_{off} = 1/t_{off}\exp(f/f_\beta)$, the bond strength f^* is exactly proportional to the logarithm of loading rate, i.e., $f^* = f_\beta \log_e(r_f\, t_{off}/f_\beta)$, where the loading rate intercept $r_f(0)$ at zero force reveals the unstressed transition rate, i.e., $r_f(0)/f_\beta = 1/t_{off}$. An important corollary to this simple force spectrum for a single activation barrier is that the standard deviations in force distributions are set by the slope of the spectrum or force scale f_β in the absence of experimental error (19).

Two distinct regimes are apparent in the spectra for L-selectin bonds in Ca^{2+} (Fig. 3 *A* and *B*). Thus we matched the continuous spectrum (Eq. 2) with the data to obtain unstressed transition rates and force scales for a sequence of two energy barriers. Plotted in Fig. 3 *A* and *B*, the continuous spectrum crosses over smoothly with log(loading rate) from one regime to the next through a high-curvature bend. However, within a regime, the spectrum closely follows the linear proportionality to the logarithm of loading rate that would arise from the particular barrier alone based on its unstressed transition rate $1/t_{off}$ and thermal force scale f_β. The high-strength regimes above 10^4 pN/sec in Ca^{2+} have a common force scale of $f_\beta \approx 70$ pN, which maps a barrier close in at a distance $x_\beta \approx 0.6$Å along the direction of force. Significantly, the high-strength regimes vanished in EDTA as demonstrated in Fig. 3*C* by PSGL-1 and bsLe^X interactions with L-selectin spheres. For interactions of PSGL-1, 19FT, and bsLe^X with L-selectin on spheres as well as 19FT with L-selectin on PMNs, the Ca^{2+}-dependent barrier is characterized by a very rapid unstressed transition rate of ≈100 per sec. Thus the Ca^{2+}-dependent barrier can impede dissociation and augment bond strength only under very fast speeds of loading. Although forces follow the same proportionality to log(loading rate) in the high-strength regime for PSGL-1 interactions with PMNs, the data span a 2-fold range (≈50–100 per sec) in the unstressed transition rate, as bracketed by the two spectra drawn in Fig. 3*B*.

Below 10^4 pN/sec, a common low-strength regime also appears in all spectra that is described by a slope of $f_\beta = 10$ pN that maps a second barrier much farther out at $x_\beta = 4$Å along the direction of force. The outer barrier is characterized by a much slower unstressed transition rate of ≈3 per sec, which defines the apparent off-rate in the absence of force. The low-strength regime of PSGL-1 attachments to PMNs has the same slope, but again the span of the data covers a 2-fold range in the unstressed transition rate (≈1.5–3 per sec). We speculate that the 2-fold span in unstressed transition rates for PSGL-1 attachments to PMNs indicates that the homodimer often formed a zipper of two bonds to a pair of L-selectins in a cluster on the PMN surface. The rationale is that a zipper of two bonds (which break uncooperatively one after the other) has the same spectral dependence of force on loading rate as a single bond but is shifted by −log(2) along the log(loading rate) axis (21). The shift stems from the 2-fold increase in mean survival time. More significantly, the Ca^{2+}-dependent barrier was eliminated in EDTA and by the blocking antibodies (anti-PSGL-1 mAb KPL1, anti-selectin mAbs DREG 55 and DREG 200) even in Ca^{2+}. Remnants of the low-strength regime remained that were governed by the same force scale $f_\beta \approx 10$ pN (barrier location $x_\beta \approx$ 4Å) but shifted to faster loading rates (Fig. 3*C*). The forces measured in Ca^{2+} with KPL1 bound to the PSGL-1 probe or DREG 55 bound to L-selectin spheres were indistinguishable from the forces measured for PSGL-1:L-selectin and bsLe^X:L-selectin in EDTA. These weak regimes of strength extrapolate to an apparent off rate at zero force of ≈20 per sec. By comparison, the weak-strength regime measured with DREG 200 bound to L-selectin in Ca^{2+} was slightly higher in force (as seen in Fig. 3*C*) and extrapolates to a slower apparent off-rate of ≈6 per sec at zero force. However, when measured in EDTA, there were no differences in force level between any of the antibodies and the PSGL-1:L-selectin interaction alone.

From the viewpoint of biological function, the most important result is the kinetic profile obtained for dissociation of PSGL-1 bonds to L-selectin under force, which is specified by Eq. **1** with the unstressed transition rates and thermal force scales for the two barriers [i.e., $1/t_{off}(1) = 3$ per sec, $f_\beta(1) = 10$ pN; and $1/t_{off}(2) = 100$ per sec, $f_\beta(2) = 70$ pN]. Shown in Fig. 3*D*, the profile of unbinding rate versus force is precisely equivalent to the spectrum of rupture forces in Fig. 3*A* obtained under steady ramps of force. In Fig. 3*D*, we see that the lifetime of a PSGL-1 bond to L-selectin is drastically shortened by pulling force; i.e., the rate of unbinding rises rapidly from an apparent unstressed rate of ≈3 per sec to ≈2,000 per sec at ≈200 pN! Moreover, in EDTA or when blocked by KPL1 or DREG 55 in Ca^{2+}, the rate of unbinding surpasses 1,000 per sec once the force exceeds 40 pN. The rates of cell detachment observed in flow chamber experiments are also plotted in Fig. 3*D* for comparison. When monitored at normal video framing speeds of ≈30 per sec (9, 13, 14), cell detachment rates appear to reach only ≈20 per sec at 200 pN. When increased to ≈240 frames per sec (16), the rates of cell detachment are much faster but remain below 100 per sec at forces above 200 pN.

Conclusions

The most frequent rupture force versus log(loading rate) for single carbohydrate bonds to L-selectin exposes a hierarchy of two chemically distinct transition states that govern dissociation under force. Setting the scales for exponentiation of rate under force, the activation barriers are mapped to distances of ≈0.6Å and 4Å along the unbinding pathway. The inner barrier represents a Ca^{2+} clasp between a single sLe^X and the lectin domain. Although not obtained for L-selectin, the crystal structures of cocomplexes of both sLe^X and SGP-3 (an FT and fully sulfated construct of the N-terminal domain of PSGL-1) with P-selectin also reveal a single Ca^{2+} metal ion coordination bond that links the fucose of sLe^X to the lectin domain. However, there are significant differences in how each carbohydrate ligand binds to the Ca^{2+} ion (10). Most prominently, tyrosine sulfation at position 10 on SGP-3 contributes a direct binding interaction that pulls the Asn-83 to Asp-89 loop of the lectin domain into a configuration where the Asn-83 and Glu-88 residues of the loop

ligate Ca^{2+} and form hydrogen bonds to fucose. Assuming a similar scenario for L-selectin, the fact that we find no difference in the calcium-dependent transition state seems to indicate that deformation of the lectin loop plus changes in electrostatic interactions with the metal as well as changes in hydrogen bonding have compensatory affects on the enthalpic barrier responsible for the high-strength regime. With regard to tyrosine sulfation, L-selectin lacks a basic residue at position 114 needed to interact with the second tyrosine sulfate at position 7, which, with the tyrosine sulfate at position 10, was identified as a prominent mediator of interactions in the cocomplex of SGP-3 with P-selectin (10). Blocked by mAb KPL-1, it seems then that the liganding of Ca^{2+} to fucose promoted by tyrosine sulfation is crucial for high-strength attachments of PSGL-1 to L-selectin. The common elimination of the inner barrier by the mAbs KPL1, DREG 55, and DREG 200 most likely stems from local steric hindrance of Ca^{2+} ligation to fucose, given the similar weak low-strength regimes that remain. More difficult to identify, the outer transition state seems to originate from a variable array of weak (but similar) uncooperative interactions. This follows because all of the low-strength regimes in Fig. 3 *A–C* have the same slope (21). On the basis of the recent crystal structures (10), the obvious candidates are hydrogen bonds to the Gal and NeuNAc residues of sLe^X beyond the fucose ring and perhaps other interactions arising from sulfation in the tyrosine-rich region along the N-terminal domain of PSGL-1. The function of the low-strength regime arising from the outer barrier is not known because it is too weak to be defined by conventional methods. But the role of the outer barrier may be to enhance multibond recruitment interior to cell surface contacts, where bonds feel little force, and thereby strengthen adhesion.

Detaching carbohydrate–L-selectin bonds with ramps of force spanning 4 orders of magnitude in rate, we find that rates of dissociation under force increase by nearly 1,000-fold from ≈3 per sec at zero load to ≈2,000 per sec at 200 pN. Illustrated in Fig. 3*D*, perceptions of L-selectin kinetics under force and dynamic strength established by flow chamber experiments are significantly different. However, through a major increase in video speed (from frames 30 per sec to 240 per sec), a recent flow chamber study (16) has shown that L-selectin bonds dissociate much faster than concluded from earlier studies. With exposure of previously undetected events of much shorter duration, the rates appear to be approaching our force probe results. Thus it seems that transient cell attachments in flow chamber tests involve variable numbers of bonds. This is plausible because, although densities of sites (>10 per square micrometer) are low in flow chamber studies, leukocytes are flattened on temporary arrest by downward forces $f_\perp$ comparable to the bond force. Simple mechanical analysis predicts that the contact area $A_\perp$ grows initially in time as $A_\perp \approx 4r_c\,(\pi f_\perp t/\eta_c)^{1/2}$ [where $r_c \approx 4$–5 μm and $\eta_c \approx 100$ N-sec/m^2 for PMN radius and apparent viscosity (32)] and approaches the static limit of $A_\perp \approx f_\perp/p_c$ [where $p_c \approx 10$ N/m^2 for PMN turgor pressure (32)]. Thus, contact areas of a few square micrometers can occur in a millisecond with many sites for binding. Moreover, theory shows that multiply bonded contacts under constant force also exhibit near-exponential decay in survival over time (21).

The inner calcium-dependent barrier revealed by fast detachment of single bonds appears to make possible the high strength of PSGL-1–L-selectin attachments needed to initiate cell tethering and interrupt translocation in flow. However, a single PSGL-1 attachment to L-selectin can sustain high strength only on time frames for loading of less than 0.01 sec; additional bonds would be needed for longer residence at vessel walls in conditions of high shear. Hence it seems likely that multibond recruitment is more significant in selectin-mediated function than previously appreciated and may account for the need for a complex hierarchy of inner and outer activation barriers.

This work was supported by subcontracts to E.E. from National Institutes of Health Grants HL31579 and HL54700 and by National Institutes of Health Grant GM59100 (to D.H.). S.S. is an Established Investigator of the American Heart Association and is supported by National Institutes of Health Grant AI47294.

1. Lawrence, M. B. & Springer, T. A. (1991) *Cell* **65,** 859–873.
2. von Andrian, U. H., Chambers, J. D., McEvoy, L. M., Bargatze, L. M., Arfors, K. E. & Butcher, E. C. (1991) *Proc. Natl. Acad. Sci. USA* **88,** 7538–7542.
3. Springer, T. A. (1990) *Nature (London)* **346,** 425–434.
4. Springer, T. A. (1994) *Cell* **76,** 301–314.
5. Sassetti, C., Tangemann, K., Singer, M. S. Kershaw, D. B. & Rosen, S. D. (1998) *J. Exp. Med.* **187,** 1965–1975.
6. Sako, D., Chang, X.-J., Barone, K. M., Vachino, G., White, H. M., Shaw, G., Veldman, G. M., Bean, K. M., Ahern, T. J., Furie, B., *et al.* (1993) *Cell* **75,** 1179–1186.
7. Foxall, C., Watson, S. R., Dowbenko, D., Fennie, C., Lasky, L. A., Kiso, M., Hasegawa, A., Asa, D. & Brandley, B. K. (1992) *J. Cell Biol.* **17,** 895–902.
8. Sako, D., Comess, K. M., Barone, K. M., Camphausen, R. T., Cumming, D. A. & Shaw, G. D. (1995) *Cell* **83,** 323–331.
9. Ramachandran, V., Nollert, M. U., Qui, H., Liu, W.-J., Cummings, R. D., Zhu, C. & McEver, R. P. (1999) *Proc. Natl. Acad. Sci. USA* **96,** 13771–13776.
10. Somers, W. S., Tang, J., Shaw, G. D. & Camphausen, R. T. (2000) *Cell* **103,** 467–479.
11. Kaplanski, G., Farnarier, C., Tissot, O., Pierres, A., Benoliel, A.-M., Alessi, M.-C., Kaplanski, S. & Bongrand, P. (1993) *Biophys. J.* **64,** 1922–1933.
12. Alon, R., Hammer, D. A. & Springer, T. A. (1995) *Nature (London)* **374,** 539–542.
13. Alon, R., Chen, S., Puri, K. D., Finger, E. B. & Springer, T. A. (1997) *J. Cell Biol.* **138,** 1169–1180.
14. Alon, R., Chen, S., Fuhlbrigge, R. C., Puri, K. D. & Springer, T. A. (1998) *Proc. Natl. Acad. Sci. USA* **95,** 11631–11636.
15. Brunk, D. K., Goetz, D. J. & Hammer, D. A. (1996) *Biophys. J.* **71,** 2902–2907.
16. Smith, M. J., Berg, E. L. & Lawrence, M. B. (1999) *Biophys. J.* **77,** 3371–3383.
17. Bell, G. I. (1978) *Science* **200,** 618–627.
18. Fritz, J., Katopodis, A. G., Kolbinger, F. & Anselmetti, D. (1998) *Proc. Natl. Acad. Sci. USA* **95,** 12283–12288.
19. Evans, E. & Ritchie, K. (1997) *Biophys. J.* **72,** 1541–1555.
20. Evans, E. (1998) *Faraday Discuss. Chem. Soc.* **111,** 1–16.
21. Evans, E. (2001) *Annu. Rev. Biophys. Biomol. Struct.* **30,** 105–128.
22. Merkel, R., Nassoy, P., Leung, A., Ritchie, K. & Evans, E. (1999) *Nature (London)* **397,** 50–53.
23. Ludwig, F. & Evans, E. (2000) *Boehringer Ingelheim Fonds Futura* **15,** 96–103.
24. Rief, M., Gautel, M., Osterhelt, F., Fernandez, J. M. & Gaub, H. E. (1997) *Science* **276,** 1109–1112.
25. Oberhauser, A. F., Marszalek, P. E., Erickson, H. P. & Fernandez, J. M. (1998) *Nature (London)* **393,** 181–185.
26. Strunz, T., Oroszlan, K., Shafer, R. & Guntherodt, H.-J. (1999) *Proc. Natl. Acad. Sci. USA* **96,** 11277–11282.
27. Baumgartner, W., Hinterdorfer, P., Ness, W., Raab, A., Vestweber, D., Schindler, H. & Drenckhahn, D. (2000) *Proc. Natl. Acad. Sci. USA* **97,** 4005–4010. (First Published April 4, 2000; 10.1073/pnas.070052697)
28. Evans, E., Ritchie, K. & Merkel, R. (1995) *Biophys. J.* **68,** 2580–2587.
29. Snapp, K. R., Ding, H., Atkins, K., Warnke, R., Luscinskas, F. W. & Kansas, G. S. (1998) *Blood* **91,** 154–164.
30. Fu, H., Berg, E. L. & Tsurushita, N. (1997) *Immunol. Lett.* **59,** 71–77.
31. Kramers, H. A. (1940) *Physica (Utrecht)* **7,** 284–304.
32. Evans, E. & Yeung, A. (1989) *Biophys. J.* **56,** 151–160.